Research on SVPWM and Midpoint Potential Balancing Algorithm of Improved NPC Three-Level Inverter

Deng Pan*, Jun Gao and Yicai Liu
Wuhan Business University, Wuhan 430056, Hubei, China

Keywords: 24 Sectors, Modulation Method, Estimation-Simulation-Correction, Adjustment Factor, Balancing Algorithm, Midpoint Potential.

Abstract: The traditional NPC three-level inverter SVPWM control adopts a 36-sector seven-segment modulation method, which involves a large number of trigonometric functions and coordinate transformations. This paper proposes a improved control strategy using 24 sectors, and introduces the SVPWM modulation method and implementation steps in detail. Compared with the 36-sector control method, the workload of calculation and table checking is significantly reduced. At the same time, this paper proposes a simple "estimation-simulation-correction" midpoint potential balance control algorithm, through a large number of simulation verification, extract the best adjustment factor k to adjust the action time of the starting negative small vector and the redundant small vector, and realize the balance control of the midpoint potential. Finally, the correctness of the proposed control method is verified by Simulink simulation.

1 INTRODUCTION

Medium and low voltage AC motor speed regulation system generally adopts two-level inverter topology, with SVPWM modulation technology for motor stator flux tracking, the method is easy to implement by digital controller, compared with traditional SPWM technology, The output current waveform is better, and the voltage output of the inverter link is relatively stable. Since the maximum withstand voltage value of a single MOSFET switch transistor is generally not high (≤600V). In the field of medium and high voltage and high power,three-level inverter topology is adopted, With the help of SVPWM modulation technology，the output level number increases and the output waveform quality is higher. In addition, the three-level inverter topology has less voltage switching stress for a single switch tube (Zhang, 2020; Li, 2016; Yang, 2018).

The implementation steps of the three-level inverter topologySVPWM algorithm are the division of large and small sectors, the judgment of the switching vector action sequence of each sector, the calculation of the switching vector action time, and the calculation of modulation fuze value. Model establishment relies on a large number of trigonometric operations and table queries (Li, 2016; Yang, 2018), and the frequent operation of the switch tube will increase the disturbance of the system, resulting in a decrease in control performance and an increase in the harmonic component of the output waveform (Zhang, 2020). Literature (Zhang, 2020) proposes an improved 36-sector seven-segment modulation method, which uses the coordinate translation method to correct the reference voltage vector, but due to the large number of sectors, the overall calculation amount is large.Literature (Wang, 2022) proposes a transformation method for split-inductive three-level inverter.It reduces the performance impact of short circuits on the circuit.Literature (Zhao, 2008) introduces a three-level inverter SVPWM method in 60° coordinate system, which reduces sector judgment and trigonometric operation from 36 sectors to 24 sectors, saving the operation time, However, there are few textual descriptions of the pulse-width modulation strategy of the above methods. Literature (Wang, 2010) introduces an LCL filter design method, The total inductance value of the LCL filter can be determined by the power supply power conditions and ripple suppression requirements, and on this basis, the inductance ratio and filter capacitance value can be determined. The NPC three-level topology has the problem of midpoint potential imbalance, which is a difficult point to study the structure. Literature (Song, 2004) provides a

Pan, D., Gao, J. and Liu, Y.
Research on SVPWM and Midpoint Potential Balancing Algorithm of Improved NPC Three-Level Inverter.
DOI: 10.5220/0012142200003562
In *Proceedings of the 1st International Conference on Data Processing, Control and Simulation (ICDPCS 2023)*, pages 5-16
ISBN: 978-989-758-675-0

potential control method for injecting zero vector, due to the different zero vector injection order in different sectors, This method needs to first determine the sector number, and then look up the table to obtain the zero vector action time. Literature (Fan, 2015) proposes to use optimization of the last three virtual vectors to control the midpoint potential balance. This method adopts more approximation processing in the process of virtual vector calculation, the cumulative error is large. Literature (Ovalle, 2017) proposes to use two adjacent small vectors to equivalently synthesize medium vectors to adjust the action time of small vectors and redundant small vectors. However, the synthesized medium vector is composed of asymmetric small vectors, and the influence of small vectors on the midpoint potential cannot be ignored. Literature (Song, 2012) provides a closed-loop bidirectional buck-boost converter to compensate for the impact of load disturbance on the DC side voltage, which is theoretically mature. However, BUCK/BOOST circuits need to be added, and hardware and maintenance costs increase.

This paper proposes an SVPWM control algorithm based on 24-sector improved NPC three-level inverter, and introduces the SVPWM modulation method and implementation steps in detail.At the same time, a simple "Estimation-simulation-correction" midpoint potential balance algorithm is proposed, and the optimal regulatory factor is extracted as the input quantity for the time control of the initial negative small vector and the redundant small vector through a large number of simulation verification. Finally, simulation is carried out to verify the correctness of the above algorithm and control strategy.

2 NPC THREE-LEVEL CIRCUIT TOPOLOGY ANALYSIS

Figure 1 shows the topology diagram of the NPC three-level circuit,Figure V_{dc} is the DC-side supply voltage,C_1 and C_2 are the DC side regulator capacitor, D_5、D_6、D_{11}、D_{12}、D_{17}、D_{18} are clamp diode for A、B、C phase. Sa_1~Sa_4、Sb_1~Sb_4、Sc_1~Sc_4 are switch tubes,o is the neutral point on the DC side.Since the regulator capacitors C1 and C2 are equal, so there is $Uc_1 = Uc_2 = \frac{1}{2}V_{dc}$.

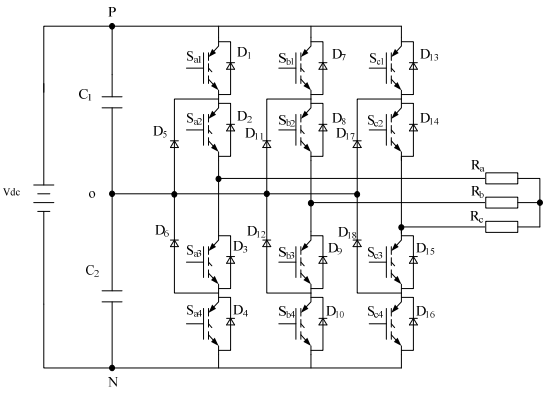

Figure 1: NPC three-level circuit topology diagram.

Each phase bridge arm can output three different levels,Define S_a、S_b、S_c as three-leg switch state variables,Take phase A as an example, S_{a1}、S_{a2} conduction, S_{a3}、S_{a4} disconnection,$U_a = \frac{1}{2}V_{dc}$, $S_a = 1$; S_{a2}、S_{a3} conduction, S_{a1}、S_{a4} disconnection, $U_a = 0$, $S_a = 0$; S_{a1}、S_{a2}disconnection,S_{a3}、S_{a4} Conduction, $U_a = -\frac{1}{2}V_{dc}$, $S_a = -1$,And S_{a1} and S_{a3} are in opposite states; S_{a2} and S_{a4} are in opposite states.

The output state of bridge arms A、B、C is represented by switch function, Define three-phase voltage as (Liu, 2012; Dang, 2016):

$$U_a = \frac{V_{dc}}{2}S_a;\ U_b = \frac{V_{dc}}{2}S_b;\ U_c = \frac{V_{dc}}{2}S_c \tag{1}$$

Equal amplitude transformation of three-phase synthetic voltage vector, And expansion by Euler formula:

$$U = \frac{2}{3}\left[U_a + U_b e^{j\frac{2}{3}\pi} + U_c e^{-j\frac{2}{3}\pi}\right] = \frac{V_{dc}}{6}[(2S_a - S_b - S_c) + j\sqrt{3}(S_b - S_c)] \tag{2}$$

Combined (1, 2), 27 kinds of space voltage vectors can be obtained, As shown in Figure 2. Four voltage vectors can be obtained by ordering the vector amplitude from large to small.

(1) The amplitude of large vector is $\frac{2}{3}V_{dc}$, For example:1 -1 -1;

(2) The amplitude of Medium vector is $\frac{\sqrt{3}}{3}V_{dc}$, For example:1 0 -1;

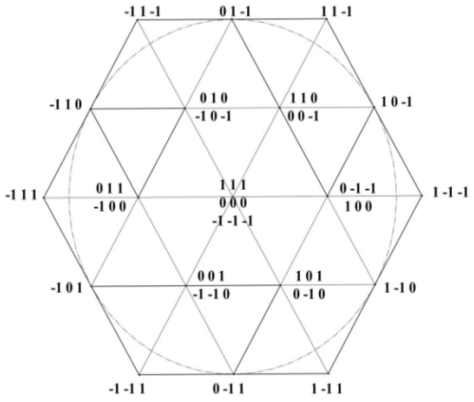

Figure 2: Basic vector diagram of NPC three-level inverter.

(3) The amplitude of Small vector is $\frac{1}{3}V_{dc}$, Small vectors are divided into positive small vectors and negative small vectors. For example, 1 0 0 is a positive small vector, 0 -1 -1 is a negative small vector;

(4) The zero vector amplitude is 0, such as 1 1 1 (Hu, 2017; Zhang, 2018; Wang, 2002).

3 ANALYSIS OF CONTROL ALGORITHM BASED ON 24 SECTORS

3.1 Division of Large and Small Sectors

In order to guide the target flux to form a quasi circular track, the voltage vector should be switched to the appropriate sector at an appropriate time, and the sector number must be agreed first.Through Clarke transformation, three-phase static A、B、C coordinate systems can be converted to two-phase static α、β coordinate systems, As shown in Figure 3.The components U_a、U_b、U_c of the rotation vector on the A、B、C axes can be represented by the components U_α、U_β of the reference vector in the two-phase stationary coordinate system.

Define variables a、b、c,And make rules:

(1) If $U_\beta > 0$, $a = 1$, otherwise $a = 0$;

(2) If $\sqrt{3}U_\alpha - U_\beta > 0$, $b = 1$, otherwise $b = 0$;

(3) If $-\sqrt{3}U_\alpha - U_\beta > 0$, $c = 1$, otherwise $c = 0$;

Define N as the large sector code, Take $N = A + 2B + 4C$, Table 1 shows the numbering rules of large sectors (Zhang, 2018; Wang, 2002).

Table 1: Table of large sector numbering sequences.

Large sector	1	2	3	4	5	6
a	1	0	1	0	1	0
b	0	1	1	0	0	1
c	0	0	0	1	1	1

Each large sector can be equally divided into four small sectors, and n is defined as the number of small sectors, As shown in Figure 4,That is, 11~14 sectors, 21~24 sectors, 31~44 sectors, 41~44 sectors, 51~54 sectors, 61~64 sectors, A total of 24 small sectors.Next, It is necessary to determine the position relationship between the target vector $\vec{V}_{ref}$ and the small sector.Taking the third sector as an example, define the included angle between $\vec{V}_{ref}$ and α axis as θ,Then the component of $\vec{V}_{ref}$ on coordinate axis α、β is:

$$\begin{cases} V_\alpha' = V_{ref} \times cos\,\theta \\ V_\beta' = V_{ref} \times \sin\theta \end{cases} \quad (3)$$

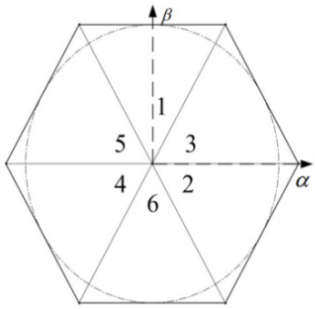

Figure 3: Large sector numbering chart.

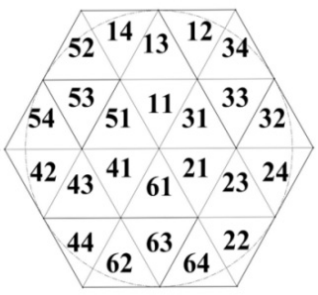

Figure 4: Small sector numbering diagram.

Table 2: Table of voltage vector action order of small sectors.

Small Sector	$T_0/4$	$T_1/2$	$T_2/2$	$T_0/2$	$T_2/2$	$T_1/2$	$T_0/4$
31	0 -1 -1	0 0 -1	0 0 0	1 0 0	0 0 0	0 0 -1	0 -1 -1
32	0 -1 -1	1 -1 -1	1 0 -1	1 0 0	1 0 -1	1 -1 -1	0 -1 -1
33	0 -1 -1	0 0 -1	1 0 -1	1 0 0	1 0 -1	0 0 -1	0 -1 -1
34	0 0 -1	1 0 -1	1 1 -1	1 1 0	1 1 -1	1 0 -1	0 0 -1

It is easy to get the judgment conditions:(1) $V'_\alpha + \frac{\sqrt{3}}{3}V'_\beta < \frac{U_{dc}}{3}$, $n = 31$; (2) $V'_\alpha - \frac{\sqrt{3}}{3}V'_\beta > \frac{U_{dc}}{3}$, $n = 32$; (3) $V'_\beta > \frac{\sqrt{3}V_{dc}}{6}$, $n = 34$; (4)Otherwise, $n = 33$. For the other five large sectors, when judging the corresponding small sector, it is only necessary to convert angle a to sector 3.

3.2 Determine the Switching Sequence of Small Sectors

The operation rule of SVPWM is to determine the three basic output space vectors according to the space sector position of target voltage vector $\vec{V}_{ref}$, and calculate the action time of each basic vector.In order to reduce the voltage stress of the switch as much as possible, the adjacent negative small vector of voltage vector $\vec{V}_{ref}$ is preferred as the starting vector. According to the above rules, the basic voltage vector of each small sector and the vector action sequence are shown in Table 2 (only the switching sequence of the third largest sector is listed in the table, see Appendix 1 for details).If the target voltage vector $\vec{V}_{ref}$ is in sector 31, the three basic vectors selected for synthesis are 0 -1 -1、0 0 -1、0 0 0.The action time of each basic vector is $\frac{T_0}{4}$、$\frac{T_1}{2}$、$\frac{T_2}{2}$、$\frac{T_0}{2}$、$\frac{T_2}{2}$、$\frac{T_1}{2}$、$\frac{T_0}{4}$.

3.3 Determine the Action Time of Three Basic Vectors

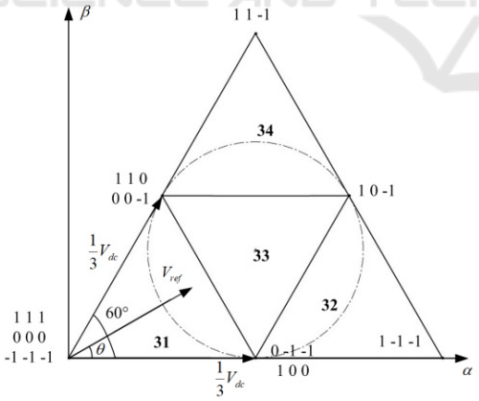

Figure 5: Third largest sector.

Take 31 sectors for example, The three basic voltage vectors of the synthetic target voltage vector $\vec{V}_{ref}$ are defined as $\vec{V}_0$、$\vec{V}_1$、$\vec{V}_2$, T_0、T_1、T_2 is the base vector response time, T_{sw} is the sampling period,From the principle of volt-second balance:

$$\begin{cases} \vec{V}_0 T_0 + \vec{V}_1 T_1 + \vec{V}_2 T_2 = \vec{V}_{ref} T_{sw} \\ T_0 + T_1 + T_2 = T_{sw} \end{cases} \tag{4}$$

31 Sector Base Vector Voltage:

$$V_0 = 0, V_1 = \frac{1}{3}V_{dc}, V_2 = \frac{1}{3}V_{dc}e^{j\frac{1}{3}\pi} \tag{5}$$

The combination formula (4, 5) yields:

$$0 + \frac{1}{3}V_{dc}T_1 + \frac{1}{3}V_{dc}e^{j\frac{1}{3}\pi}T_2 = V_{dc}e^{j\theta}T_{sw} \tag{6}$$

$$m = \frac{4}{\sqrt{3}} \times \frac{V_{ref}}{\frac{2}{3}V_{dc}} \times T_{sw}$$

Define intermediate variables ,

It can be solved:

$$\begin{cases} T_0 = m\,sin(60 - \theta) \\ T_1 = m\,sin\,\theta \\ T_2 = T_{sw} - m\,sin(\theta + 60) \end{cases} \tag{7}$$

Similarly, the basic vector action time for each small sector can be solved as shown in Table 3 (only the basic vector action time for the third largest sector is listed in the table, See Appendix 2 for details):

Table 3: Timeline of basic vector action for each sector.

Small sector	T_0 Time of action	T_1 Time of action	T_2 Time of action
31	$m\,sin(60-\theta)$	$m\,sin\,\theta$	$T_{sw}-m\,sin(60+\theta)$
32	$2T_{sw}-m\,sin(60+\theta)$	$T_{sw}-m\,sin(60-\theta)$	$m\,sin\,\theta$
33	$T_{sw}-m\,sin\,\theta$	$T_{sw}-m\,sin(60-\theta)$	$-T_{sw}+m\,sin(60+\theta)$
34	$m\,sin(60-\theta)$	$-T_{sw}+m\,sin\,\theta$	$2T_{sw}-m\,sin(60+\theta)$

3.4 Determine Switch Fuse Value

In order to minimize the harmonic component of the output voltage of the inverter, a seven-segment symmetric SVPWM modulation is usually used, that is, the inverter outputs seven voltage vectors in one switch cycle (Song, 2012). Figure 6 shows a method to determine the switch start time. An isosceles triangle is generated by the counter and compared with a constant value to determine the switch time. The constant value mentioned here is the switch fuse value.

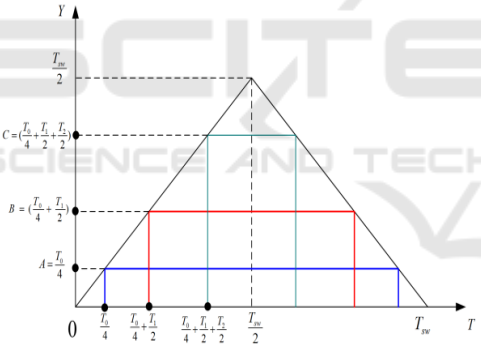

Figure 6: The corresponding diagram of the switching time.

The seven time periods in the figure correspond to six switch moments. The input moments of each vector can be obtained by comparing the three switch fuses A、B、C in the figure with the triangular wave.The amplitude of the triangle wave in the graph is set to $\frac{T_{sw}}{2}$, Period set to T_{sw}.When the projection value of the triangular wave output on the Y axis is in the range of 0-A, the corresponding vector trigger time is $\frac{T_0}{4}$.When the projection value is within $A\sim B$ range, the corresponding vector trigger time is $(\frac{T_0}{4}+\frac{T_1}{2})$, When the projection value is within $B\sim C$ range, the corresponding vector trigger time is $(\frac{T_0}{4}+\frac{T_1}{2}+\frac{T_2}{2})$,Therefore, the value of A、B、C should meet the following relationship:

$$\begin{cases} A=\frac{T_0}{4} \\ B=A+\frac{T_1}{2}=\frac{T_0}{4}+\frac{T_1}{2} \\ C=B+\frac{T_2}{2}=\frac{T_0}{4}+\frac{T_1}{2}+\frac{T_2}{2} \end{cases} \quad (8)$$

Taking three sectors as an example, the comparison relationship between the basic vector action time and the switch state is shown in Figure 7. The three-phase vector state corresponds to all the switch states. The switching on and off times of the switch devices are allocated to the corresponding switch devices to complete the selection of the main circuit switch devices.

Table 4 shows the trigger time table of switching devices in each small sector (only the third largest sector is taken as an example in the table, see Appendix 3 for details).Define variable $X=\frac{T_0}{4}, Y=\frac{T_0}{4}+\frac{T_1}{2}, Z=\frac{T_0}{4}+\frac{T_1}{2}+\frac{T_2}{2}$, As the switch status of the bridge arms of each phase is opposite to each other, the table only lists the trigger time of the two switches on the upper layer of each bridge arm.In addition, if the state value in the table is 1, it means that the switch cycle is high level, otherwise it is low level.

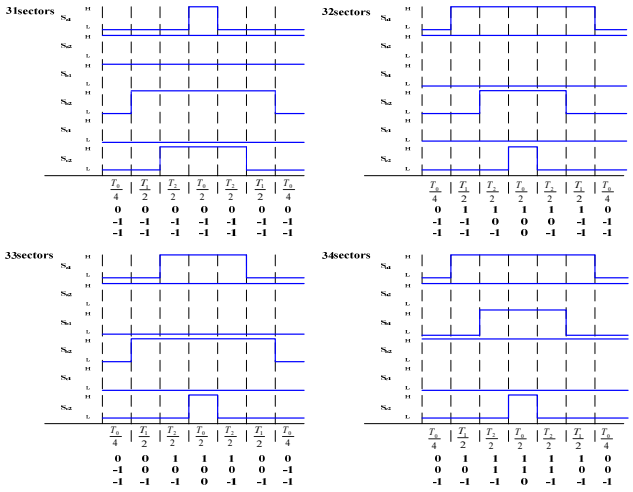

Figure 7: Seven-segment SVPWM modulation waveform (taking sector 3 as an example).

Table 4: Switching device trigger schedules for each sector.

n	S_{a1}	S_{a2}	S_{b1}	S_{b2}	S_{c1}	S_{c2}
31	Z	1	0	X	0	Y
32	X	1	0	Y	0	Z
33	Y	1	0	X	0	Z
34	X	1	Y	1	0	Z

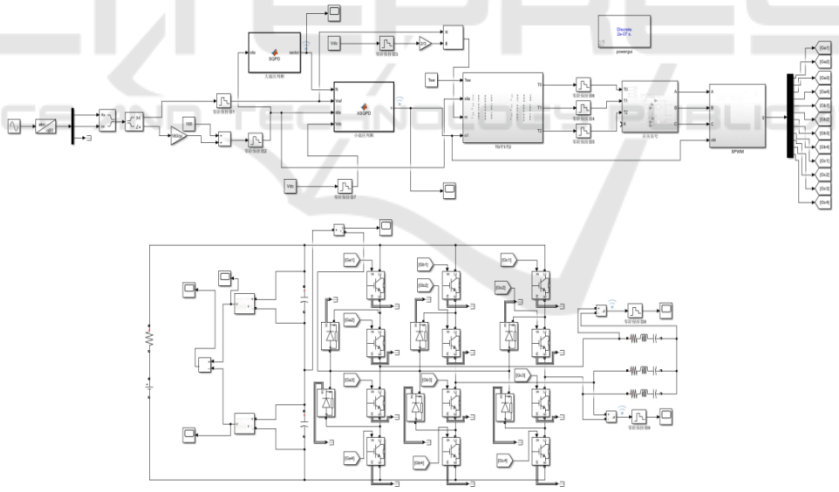

Figure 8: SVPWM control simulation model of a 24-sector NPC three-level inverter.

3.5 Simulation Verification

The simulation model built by Simulink is shown in Figure 8, and the parameter settings are as follows: the DC side voltage of the inverter V_{dc} is 500V, the expected inverter output a rotation voltage vector with a period of 0.02s and amplitude of 180V, and the defined cycle sampling frequency F_{sw} is 1e4Hz, and the sampling period T_{sw} is 1e-4s; The three-phase symmetrical load resistance is 100Ω, the inductance L is 16e-6H, and the capacitance C is 16e-6F;The DC side voltage stabilizing capacitor C_1、C_2 is 500e-6F.Powergui adopts Discrete mode, and the system sampling frequency is set to 20 times of the periodic sampling frequency.

```
大扇区判断
function sector = SQPD(sita)%判断大扇区
sector=0;
    if(floor(sita/60)==0)
        sector=3;
    elseif(floor(sita/60)==1)
        sector=1;
         elseif(floor(sita/60)==2)
        sector=5;
     elseif(floor(sita/60)==3)
        sector=4;
          elseif(floor(sita/60)==4)
        sector=6;
    else
        sector=2;

    end
```

```
function n = XSQPD(N,Vref,sita,Vdc)%判断小扇区
n=0;
switch N
    case 3
    Valpa=Vref*cos(sita);
    Vbeta=Vref*sin(sita);
    if(Valpa+sqrt(3)/3*Vbeta<=Vdc/3)
        n=31;
    elseif(Valpa-sqrt(3)/3*Vbeta>=Vdc/3)
        n=32;
         elseif(Vbeta>sqrt(3)/6*Vdc)
        n=34;
    else
        n=33;
    end
```

Figure 9: S-Function is used to determine large and small sectors.

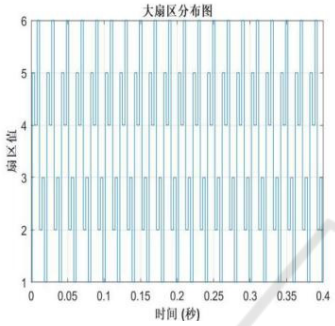

Figure 10: Distribution of large sectors.

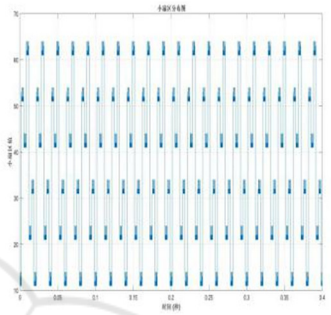

Figure 11: *Distribution of small sectors.*

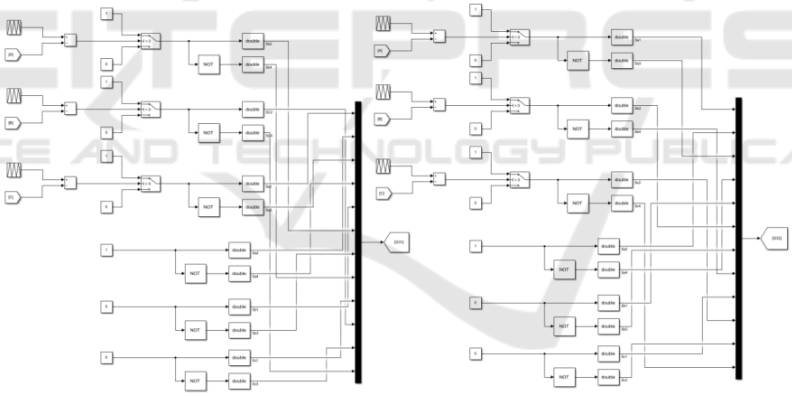

Figure 12: Sectors 31 and 32 judge the switching time

The S-Function function is used to judge the large and small sectors, as shown in Figure 9. For the judgment of small sectors, only the judgment method of the third sector is listed in the figure, and the judgment method of other sectors is the same. Figure 10 and Figure 11 show the distribution of large and small sectors after operation.

Figure 12 shows the judgment statement for the trigger time of sector 31 and 32 switches. The three-level SVPWM modulation trigger pulse can be obtained by comparing the switch fuse value with the Y-axis projection value of the modulated triangle wave and strictly comparing the trigger schedule of the switching devices in each sector (Appendix 3). Set the simulation environment of Simulink. The simulation start time is 0s and the end time is 0.4s. Fixed step is adopted and Discrete mode is adopted for the algorithm.

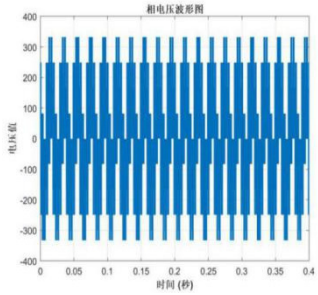

Figure 13: Load phase voltage waveform

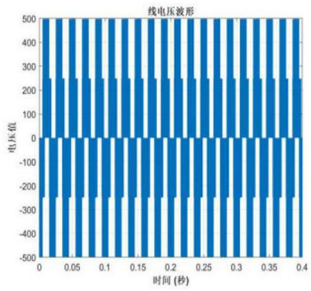

Figure 14: Load line voltage waveform.

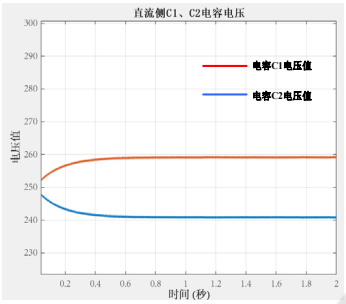

Figure 15: Capacitor C1 and C2 voltage values.

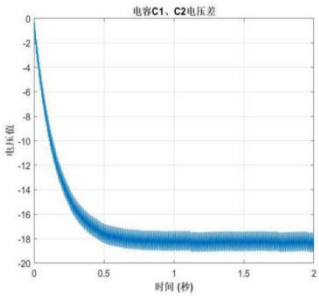

Figure 16: Voltage difference between capacitors C1 and C2.

Figure 13 and Figure 14 are waveform diagrams of three-phase load phase voltage and line voltage respectively. The waveform period is 0.02s, in which the amplitude of phase voltage is $\frac{2}{3}V_{dc}$, and there are $\frac{1}{3}V_{dc}$ and $\frac{\sqrt{3}}{3}V_{dc}$ voltage vectors in the waveform; The line voltage amplitude is V_{dc}, and there are V_{dc} and $\frac{1}{2}V_{dc}$ voltage vectors in the waveform. The simulation waveform further verifies the conclusion in 2.1.

4 A SIMPLE MIDPOINT POTENTIAL BALANCE ALGORITHM BASED ON "ESTIMATION-SIMULATION-CORRECTION"

Further verify the influence of the above SVPWM algorithm on the neutral point potential of the inverter. Measure the two capacitor voltages and the neutral point voltage of the DC bus respectively, extend the simulation time to 2s, and obtain curves as shown in Figures 15 and 16. After the simulation starts, the voltage values of C_1、C_2 capacitors are roughly the same, the midpoint voltage is about 0V, and there is almost no zero shift at the moment of starting. The simulation lasts for 0.5s, the voltage value of C_1 capacitor is about 260V, the voltage value of C_2 capacitor is about 240V, The differential pressure at both ends of capacitor C_1 and C_2 is about 20V. As time goes on, the offset of the midpoint voltage increases, and the distortion of the line voltage is obvious, which will interfere with the steady state performance of the system (Fan, 2015; Dang, 2016). When paired small vectors act on the midpoint, they produce the same line voltage, but their current values have the opposite effect on the midpoint voltage, counteracting part of the voltage imbalance (Zhang, 2018). To achieve a balanced control of the midpoint potential, the action time of negative small vectors and redundant small vectors can be allocated (Jiang, 2014). An adjusting factor k is introduced to modify the on-off fuse of the starting negative and redundant small vectors, thus changing the on-off time of the switch tube.

Analyzing Figure 1, when the current flows into the bus, when $i<0$, C_1 is discharged, and C_2 is charged, the midpoint potential has an upward trend; Conversely, $i>0$, C_1 charge, C_2 discharge, midpoint potential has a downward trend (Song, 2004). The S-Function function is used to determine the value of the pair, and the input amount is the voltage difference of capacitors C_1、C_2 (V_{12} in the figure) and the current flowing in/out of the DC bus.

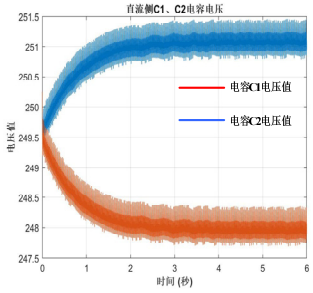

Figure 17: The value of the capacitor voltage.

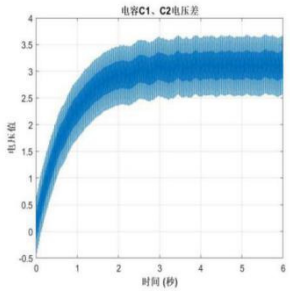

Figure 18: Capacitor voltage difference.

The method of "Estimation-simulation -correction" is adopted, and different parameters are estimated respectively, verified by a large number of simulations, and the obtained values are corrected.

The simulation results show that when $i>0$ and $V_{12}>0$, $k=0.7$; when $i>0$ and $V_{12}<0$, $k=0.3$; when $i<0$ and $V_{12}>0$, $k=0.3$; when $i<0$ and $U_{12}<0$, $k=0.7$, In this way, the offset suppression effect of the midpoint voltage of the DC bus is better. After the k value is introduced, equation (8) is modified to obtain an optimized switch fuze as shown in equation (9):

$$\begin{cases} A=\frac{T_0}{4}\times \ （1+0.7） \\ B=A+\frac{T_1}{2}=\frac{T_0}{4}+\frac{T_1}{2} \\ C=B+\frac{T_2}{2}=\frac{T_0}{4}\times(1-0.7)+\frac{T_1}{2}+\frac{T_2}{2} \end{cases} \quad (9)$$

Modify the model parameters according to equation (9), and the simulation time is extended to 6s, and the voltage difference and midpoint voltage waveform of the DC bus capacitor are shown in Figures 17 and 18. In Figure 17, the stability value of the DC side power supply C_1 is about 251V, the stability value of C_2 is about 248V, and the voltage difference between the readout capacitors C_1、C_2 in Figure 18 is about 3V, and it tends to stabilize over time, The simple algorithm better suppresses the fluctuation of midpoint potential.

5 CONCLUSION

Based on the traditional 36 sector SVPWM control algorithm, this paper proposes an improved 24 sector SVPWM control algorithm, and introduces the modulation method and implementation steps of this algorithm in detail. At the same time, a simple "Estimation-simulation-correction" neutral point potential balance control algorithm is proposed, and the value method of regulating factor k is introduced, as well as how to use the value of k to allocate the action time of negative small vectors and redundant small vectors. A simulation model is built to verify the above algorithm. Combined with the simulation results, the correctness of the proposed control algorithm is proved.

ACKNOWLEDGEMENT

Fund: Wuhan Business College University-level Scientific Research Project (2021KY017).

REFERENCES

Zhang Yunlei, Wang Qunjing, Hu Cungang, et al. Research on a new low-voltage non isolated 17 level converter and its control strategy. *Chinese Journal of Electrical Engineering*, 2020, 40(4):1095-1105.

KAI Li, ZHAO Jiancheng,WU Wenjie. Performance analysis of zero common-mode voltagepulse-width modulation techniques for three - level neutral point clamped inverters. *IET Power Electronics*, 2016, 9(14):2654-2664.

Yang Yun,Tan Siew-Chong,Hui Shu Yuen Ron. Adaptive reference model predictive control with improved performance for voltage-source inverters. *IEEE Trans on Control Systems Technology*, 2018, 26(2): 724-731.

Wang Xiaobiao, Xiao Huaping, Niu Chenhui, Yao Zhongyuan, Xiao Huafeng. Research on the construction method of highly reliable three-level inverter. *Chinese Journal of Electrical Engineering*, 2022, 25 (4):839-849.

Song Qiang, Liu Wenhua, Yan Gangui, Wang Zhonghong. Neutral point potential balance control method of three-level NPC inverter based on zero sequence voltage injection. *Chinese Journal of Electrical Engineering*, 2004, 05(6):52-62.

Zhao Hui, Li Rui, Wang Hongjun, Yue Youjun. Research on SVPWM method of three-level inverter in 60°coordinate system. *Chinese Journal of Electrical*

Engineering, 2008, 30(5):405-413.

Wang Fusheng, Shao Zhang, Ping Liuping. Current ripple analysis and LCL filter design of three-level inverter. *Power Electronics Technology*, 2010, 44(11):76-84.

Ovalle A., Hernández M. E. Nonorthogonal-Reference-Frame-Based SVPWM Framework for Multilevel Inverters. *IEEE Transactions on Power Electronics*, 2017, 32(6):4925-4938.

Fan Bo, Zhao Weigang, Liu Gang, Xie Dongdong Closed loop control of neutral point potential balance of three-level inverter based on optimized virtual vector. *Journal of Electrical Technology*, 2015, 30(04):124-132.

Song Wensheng, Feng Xiaoyun. Internal relationship between a single-phase three-level SVPWM modulation and carrier SPWM. *Journal of Electrical Technology*, 2012, 27(6):131-138.

Jiang Haipeng, Liu Yongqiang. Simplified SVPWM double closed loop control of VIENNA rectifier with neutral point potential balance control. *Journal of Motor and Control*, 2014, 18(2):35-41. DOI: 10.15938/2014.02.007.

Liu Sensen, Li Bin, Hang Lijun, etc A new control method of VIENNA rectifier when three-phase power network is unbalanced. *Chinese Journal of Electrical Engineering*, 2012, 32(21):54-62. DOI: 10.13334/j.0258-8013. pcsee. 2012.21.009.

Dang Chaoliang, the same as Qianfeng, etc. Proportional repetitive control of Vienna rectifier based on equivalent carrier SVM. *Power Electronics Technology*, 2016, 50(12):59-62+70. DOI: CNKI: SUN: DLDZ. 0.2016-12-021.

Hu Cungang, Ma Dajun, Wang Qunjing, et al. Loss distribution balance control strategy for three-level active neutral point clamped inverter. *Journal of Electrical Technology*, 2017, 32(1):129-138.

Zhang Ming, Guo Yuanbo, Li Ze, et al. Output voltage imbalance suppression method of three-level inverter under fault tolerant control mode. *Journal of Electrical Technology*, 2018, 33(22):5300-5310.

Wang Guangzhu. Study on the unbalance mechanism of capacitor voltage on DC side of diode clamped multilevel inverter. *Chinese Journal of Electrical Engineering*, 2002, 22(12):111-117.

APPENDIX

Appendix 1: ACTION Sequence of Small Sector Voltage Vector

n	$T_0/4$	$T_1/2$	$T_2/2$	$T_0/2$	$T_2/2$	$T_1/2$	$T_0/4$	*n*	$T_0/4$	$T_1/2$	$T_2/2$	$T_0/2$	$T_2/2$	$T_1/2$	$T_0/4$
31	0-1 -1	0 0 -1	0 0 0	1 0 0	0 0 0	0 0 -1	0 -1-1	**11**	0 0 -1	0 0 0	0 1 0	1 1 0	0 1 0	0 0 0	0 0 -1
32	0-1 -1	1-1 -1	1 0 -1	1 0 0	1 0 -1	1-1 -1	0-1 -1	**12**	0 0 -1	01 -1	1 1 -1	1 1 0	1 1-1	0 1 -1	0 0 -1
33	0-1 -1	0 0 -1	1 0 -1	1 0 0	1 0 -1	0 0 -1	0-1 -1	**13**	0 0 -1	01 -1	0 1 0	1 1 0	0 1 0	0 1 -1	0 0 -1
34	0 0 -1	1 0 -1	1 1 -1	1 1 0	1 1 -1	1 0 -1	0 0 -1	**14**	-10 -1	-11-1	0 1 -1	0 1 0	0 1 -1	-11 -1	-10 -1
51	-10 -1	-10 0	0 0 0	0 1 0	0 0 0	-1 0 0	-10 -1	**41**	-1 0 0	0 0 0	0 0 1	0 1 1	0 0 1	0 0 0	-1 0 0
52	-10 -1	-11-1	-1 1 0	0 1 0	-1 1 0	-11 -1	-10 -1	**42**	-1 0 0	-10 1	-1 1 1	0 1 1	-1 1 1	-1 0 1	-1 0 0
53	-10 -1	-10 0	-1 1 0	0 1 0	-1 1 0	-1 0 0	-10 -1	**43**	-1 0 0	-10 1	0 0 1	0 1 1	0 0 1	-1 0 1	-1 0 0
54	-1 0 0	-11 0	-1 1 1	0 1 1	-1 1 1	-1 1 0	-1 0 0	**44**	-1-1 0	-1-11	-1 0 1	0 0 1	-1 0 1	-1-1 1	-1-1 0
61	-1-1 0	0 -1 0	0 0 0	0 0 1	0 0 0	0 -1 0	-1-1 0	**21**	0 -1 0	0 0 0	1 0 0	1 0 1	1 0 0	0 0 0	0 -1 0
62	-1-1 0	-1-1 1	0 -1 1	0 0 1	0 -1 1	-1-1 1	-1-1 0	**22**	0 -1 0	1-1 0	1 -1 1	1 0 1	1 -1 1	1 -1 0	0 -1 0
63	-1-1 0	0 -1 0	0 -1 1	0 0 1	0 -1 1	0 -1 0	-1-1 0	**23**	0 -1 0	1-1 0	1 0 0	1 0 1	1 0 0	1 -1 0	0 -1 0
64	0 -1 0	0 -1 1	1 -1 1	1 0 1	1 -1 1	0 -1 1	0 -1 0	**24**	0-1 -1	1-1-1	1 -1 0	1 0 0	1 -1 0	1-1 -1	0-1 -1

Appendix 2: BASIC Vector Action Schedule of Each Sector

n	Action time of T_0	Action time of T_1	Action time of T_2
31	$m\sin(60-\theta)$	$m\sin\theta$	$T_{sw}-m\sin(60+\theta)$
32	$2T_{sw}-m\sin(60+\theta)$	$T_{sw}-m\sin(60-\theta)$	$m\sin\theta$
33	$T_{sw}-m\sin\theta$	$T_{sw}-m\sin(60-\theta)$	$-T_{sw}+m\sin(60+\theta)$
34	$m\sin(60-\theta)$	$-T_{sw}+m\sin\theta$	$2T_{sw}-m\sin(60+\theta)$
11	$\frac{4}{\sqrt{3}}\bullet m\bullet T_{sw}\bullet sin(60-(\theta-60))$	$T_{sw}-\frac{4}{\sqrt{3}}\bullet m\bullet T_{sw}\bullet sin(60+(\theta-60))$	$\frac{4}{\sqrt{3}}\bullet m\bullet T_{sw}\bullet sin(\theta-60)$
12	$2T_{sw}-\frac{4}{\sqrt{3}}\bullet m\bullet T_{sw}\bullet sin(60+(\theta-60))$	$\frac{4}{\sqrt{3}}\bullet m\bullet T_{sw}\bullet sin(\theta-60)$	$T_{sw}-\frac{4}{\sqrt{3}}\bullet m\bullet T_{sw}\bullet sin(60-(\theta-60))$
13	$T_{sw}-\frac{4}{\sqrt{3}}\bullet m\bullet T_{sw}\bullet sin(\theta-60)$	$-T_{sw}+\frac{4}{\sqrt{3}}\bullet m\bullet T_{sw}\bullet sin(60+\theta-60)$	$T_{sw}-\frac{4}{\sqrt{3}}\bullet m\bullet T_{sw}\bullet sin(60-(\theta-60))$
14	$\frac{4}{\sqrt{3}}\bullet m\bullet T_{sw}\bullet sin(60-(\theta-60))1$	$2T_{sw}-\frac{4}{\sqrt{3}}\bullet m\bullet T_{sw}\bullet sin(60+(\theta-60))$	$-T_{sw}+\frac{4}{\sqrt{3}}\bullet m\bullet T_{sw}\bullet sin(\theta-60)$
51	$\frac{4}{\sqrt{3}}\bullet m\bullet T_{sw}\bullet sin(60-(\theta-120))$	$\frac{4}{\sqrt{3}}\bullet m\bullet T_{sw}\bullet sin(\theta-120)$	$T_{sw}-\frac{4}{\sqrt{3}}\bullet m\bullet T_{sw}\bullet sin(60+(\theta-120))$
52	$2T_{sw}-\frac{4}{\sqrt{3}}\bullet m\bullet T_{sw}\bullet sin(60+(\theta-120))$	$T_{sw}-\frac{4}{\sqrt{3}}\bullet m\bullet T_{sw}\bullet sin(60-(\theta-120))$	$\frac{4}{\sqrt{3}}\bullet m\bullet T_{sw}\bullet sin(\theta-120)$
53	$T_{sw}-\frac{4}{\sqrt{3}}\bullet m\bullet T_{sw}\bullet sin(\theta-120)$	$T_{sw}-\frac{4}{\sqrt{3}}\bullet m\bullet T_{sw}\bullet sin(60-(\theta-120))$	$-T_{sw}+\frac{4}{\sqrt{3}}\bullet m\bullet T_{sw}\bullet sin(60+(\theta-120))$
54	$\frac{4}{\sqrt{3}}\bullet m\bullet T_{sw}\bullet sin(60-(\theta-120))$	$-T_{sw}+\frac{4}{\sqrt{3}}\bullet m\bullet T_{sw}\bullet sin(\theta-120)$	$2T_{sw}-\frac{4}{\sqrt{3}}\bullet m\bullet T_{sw}\bullet sin(60+(\theta-120))$
41	$\frac{4}{\sqrt{3}}\bullet m\bullet T_{sw}\bullet sin(60-(\theta-180))$	$T_{sw}-\frac{4}{\sqrt{3}}\bullet m\bullet T_{sw}\bullet sin(60+(\theta-180))$	$\frac{4}{\sqrt{3}}\bullet m\bullet T_{sw}\bullet sin(\theta-180)$
42	$2T_{sw}-\frac{4}{\sqrt{3}}\bullet m\bullet T_{sw}\bullet sin(60+(\theta-180))$	$\frac{4}{\sqrt{3}}\bullet m\bullet T_{sw}\bullet sin(\theta-180)$	$T_{sw}-\frac{4}{\sqrt{3}}\bullet m\bullet T_{sw}\bullet sin(60-(\theta-180))$
43	$T_{sw}-\frac{4}{\sqrt{3}}\bullet m\bullet T_{sw}\bullet sin(\theta-180)$	$-T_{sw}+\frac{4}{\sqrt{3}}\bullet m\bullet T_{sw}\bullet sin(60+\theta-180)$	$T_{sw}-\frac{4}{\sqrt{3}}\bullet m\bullet T_{sw}\bullet sin(60-(\theta-180))$
44	$\frac{4}{\sqrt{3}}\bullet m\bullet T_{sw}\bullet sin(60-(\theta-180))$	$2T_{sw}-\frac{4}{\sqrt{3}}\bullet m\bullet T_{sw}\bullet sin(60+(\theta-180))$	$-T_{sw}+\frac{4}{\sqrt{3}}\bullet m\bullet T_{sw}\bullet sin(\theta-180)$
61	$\frac{4}{\sqrt{3}}\bullet m\bullet T_{sw}\bullet sin(60-(\theta-240))$	$\frac{4}{\sqrt{3}}\bullet m\bullet T_{sw}\bullet sin(\theta-240)$	$T_{sw}-\frac{4}{\sqrt{3}}\bullet m\bullet T_{sw}\bullet sin(60+(\theta-240))$
62	$2T_{sw}-\frac{4}{\sqrt{3}}\bullet m\bullet T_{sw}\bullet sin(60+$	$T_{sw}-\frac{4}{\sqrt{3}}\bullet m\bullet T_{sw}\bullet sin(60-$	$\frac{4}{\sqrt{3}}\bullet m\bullet T_{sw}\bullet sin(\theta-240)$

	（$\theta-240$）)	（$\theta-240$）)	
63	$T_{sw}-\frac{4}{\sqrt{3}}\bullet m\bullet T_{sw}\bullet sin$ （$\theta-240$）	$T_{sw}-\frac{4}{\sqrt{3}}\bullet m\bullet T_{sw}\bullet sin(60-$（$\theta-240$）)	$-T_{sw}+\frac{4}{\sqrt{3}}\bullet m\bullet T_{sw}\bullet sin(60+$（$\theta-240$）
64	$\frac{4}{\sqrt{3}}\bullet m\bullet T_{sw}\bullet sin(60-$（$\theta-240$）)	$-T_{sw}+\frac{4}{\sqrt{3}}\bullet m\bullet T_{sw}\bullet sin$ （$\theta-240$）	$2T_{sw}-\frac{4}{\sqrt{3}}\bullet m\bullet T_{sw}\bullet sin(60+$（$\theta-240$）
21	$\frac{4}{\sqrt{3}}\bullet m\bullet T_{sw}\bullet sin(60-$（$\theta-300$）)	$T_{sw}-\frac{4}{\sqrt{3}}\bullet m\bullet T_{sw}\bullet sin(60+$（$\theta-300$）)	$\frac{4}{\sqrt{3}}\bullet m\bullet T_{sw}\bullet sin$ （θ-300）
22	$2T_{sw}-\frac{4}{\sqrt{3}}\bullet m\bullet T_{sw}\bullet sin(60+$（$\theta-300$）)	$\frac{4}{\sqrt{3}}\bullet m\bullet T_{sw}\bullet sin(\theta-300)$	$T_{sw}-\frac{4}{\sqrt{3}}\bullet m\bullet T_{sw}\bullet sin(60-$（$\theta-300$）)
23	$T_{sw}-\frac{4}{\sqrt{3}}\bullet m\bullet T_{sw}\bullet sin(\theta-300)$	$-T_{sw}+\frac{4}{\sqrt{3}}\bullet m\bullet T_{sw}\bullet sin$ （$60+\theta-300$）	$T_{sw}-\frac{4}{\sqrt{3}}\bullet m\bullet T_{sw}\bullet sin(60-$（$\theta-300$）)
24	$\frac{4}{\sqrt{3}}\bullet m\bullet T_{sw}\bullet sin(60-$（$\theta-300$）)	$2T_{sw}-\frac{4}{\sqrt{3}}\bullet m\bullet T_{sw}\bullet sin(60+$（$\theta-300$）)	$-T_{sw}+\frac{4}{\sqrt{3}}\bullet m\bullet T_{sw}\bullet sin(\theta-300)$

Appendix 3: TRIGGER Schedule of Switching Devices in Each Sector

n	S_{a1}	S_{a2}	S_{b1}	S_{b2}	S_{c1}	S_{c2}	n	S_{a1}	S_{a2}	S_{b1}	S_{b2}	S_{c1}	S_{c2}
31	Z	1	0	X	0	Y	**11**	Z	1	Y	1	0	X
32	X	1	0	Y	0	Z	**12**	Y	1	X	1	0	Z
33	Y	1	0	X	0	Z	**13**	Z	1	X	1	0	Y
34	X	1	Y	1	0	Z	**14**	0	Y	X	1	0	Z
51	0	Y	Z	1	0	X	**41**	0	X	Z	1	Y	1
52	0	Z	X	1	0	Y	**42**	0	Z	Y	1	X	1
53	0	Z	Y	1	0	X	**43**	0	Y	Z	1	X	1
54	0	Z	X	1	Y	1	**44**	0	Z	0	Y	X	1
61	0	X	0	Y	Z	1	**21**	Y	1	0	X	Z	1
62	0	Y	0	Z	X	1	**22**	X	1	0	Z	Y	1
63	0	X	0	Z	Y	1	**23**	X	1	0	Y	Z	1
64	Y	1	0	Z	X	1	**24**	X	1	0	Z	0	Y